Spatiotemporal Step Patterns during Crystal Growth in a Transport-Controlled System

Olga Gliko and Peter G. Vekilov*

Department of Chemical Engineering, University of Houston, Houston, Texas 77204

Received: March 30, 2002; In Final Form: August 29, 2002

We aim at insight into the unsteady kinetics and the formation of spatiotemporal patterns of steps during the crystal growth in systems, in which the growth rate is controlled by the rate of supply of material. For this, we apply phase-shifting interferometry to the crystallization of the protein ferritin. We find that the locally measured growth rate, step density and step velocity fluctuate by up to 80−100% of their average values. The fluctuations are due to passage of step bunches generated at the facet edges due to unsteady surface nucleation. The fluctuation amplitudes *decrease* with higher supersaturation and larger crystal size, as well as with increasing distance from the step sources, even while the average value of local slope, a destabilizing factor, increases. Since size and supersaturation are parameters affecting the solute supply field, we conclude that fluctuations are rooted in the coupling of the interfacial processes of growth to the bulk transport in the solution. To understand the counterintuitive *suppression* of the instability, we analyzed the step velocity dependence on local slope and found only a very weak interaction between the steps, likely due to competition for supply from the solution. Accordingly, the step bunches propagate with the same velocity as elementary steps. We conclude that in transport-controlled systems with noninteracting or weakly interacting steps the stable growth mode is that via equidistant step trains, and randomly arising step bunches decay. Stronger step interactions may reverse this conclusion, or slow the rate, at which step bunches decay and stability is reached.

I. Introduction

X-ray diffraction from protein crystals is still the dominant method of determination of the atomic structure of the protein molecules.[1] It requires single crystals as large as several tenths of a millimeter with high compositional and structural uniformity.[2,3] Unsteady growth conditions and time-dependent impurity incorporation into growing crystals lead to striae and deterioration of the crystal quality.[4] Besides, inhomogenuities arise even under steady external conditions if intrinsic kinetics instabilities, such as step bunching occur;[5] bunching has been shown to cause growth striations in lysozyme crystals.[6]

The kinetics instabilities and step bunching during the crystallization of the protein lysozyme were studied using a high-resolution interferometry technique.[7] It was concluded that fluctuations are intrinsic and result from the coupled bulk transport and interfacial kinetics processes.[8,9] According to the mechanism put forth in these works, the strongest instabilities occur when the growth proceeds under equal weights of the transport and kinetics in the overall rate control. Hence, shifts toward purely kinetic, or, conversely, purely diffusive regimes should lead to higher stability. Changing the system parameters toward stronger kinetics control decreases the fluctuation amplitudes, while stronger step kinetics nonlinearities (step−step interactions, asymmetry for incorporation form the top and lower terraces,[10,11] stochastic generation of new crystalline layers, etc.) increase them.[12]

If the rationale developed based on lysozyme data holds, in crystallization systems with dominant transport control, such as ferritin, a shift of the working point toward slower transport should dampen the fluctuations. Ferritin is a suitable system for studies of nonlinear dynamics—the molecular mechanisms of ferritin crystallization and defect formation has been elucidated to a certain detail using atomic force microscopy.[13,14] Thus, the aim of the investigations discussed here is to test if ferritin growth is steady or unsteady, and if the latter, to experimentally study the origin of kinetics unsteadiness. We search the answer to this question in the dependencies of the amplitude of local slope fluctuations on the parameters affecting transport to the interface: supersaturation, crystal size, and location on the crystal faces.

II. Experimental Procedures

II.1. Solutions and Crystallization. The crystallizing solution contains between 2 and 2.5 mg/mL horse spleen ferritin purchased form Sigma and purified to reduce the level of the most common impurity, the covalent dimer of ferritin, to below 5%.[15] We use 2.0% (w/v) $CdSO_4$ as a precipitant, and 0.2 M sodium acetate buffer ($NaCH_3COO$ CH_3COOH) to fix pH at 5.05. The temperature of the solution in the growth cell is stabilized to 23 ± 0.01 °C by a thermoelectric (Peltier) cooler.[16] The supersaturation is calculated as $\sigma = \ln(\gamma C/\gamma_e C_e) \approx \ln(C/C_e)$, where C is concentration of the solution, $C_e = 35$ μg/mL [17] is solubility, and γ and γ_e are the activity coefficients at ferritin concentrations C and C_e, respectively; as shown in ref 13, $\gamma \approx \gamma_e \approx 1$.

II.2. Phase-Shifting Interferometry. We used a phase-shifting interferometry technique specifically developed for this study.[16] The phase-shifting algorithm chosen by us employs five-image sequences captured with a phase shift of $\pi/2$; digital processing of the sequence allows reconstruction of the surface morphology with a depth resolution of 5 nm across a field of view of 1 × 1 mm^2, for further details of the technique and discussion of the extensive tests and calibrations, see ref 16. The time traces of the normal growth rate R, local slope proportional to step density p, and step velocity v are recorded at select locations on the crystal surface with time resolution of 1 s. For this, the interferometric intensity records from pixels separated by 0.5−1 μm in the space of the crystal surface are

10.1021/jp025863o CCC: $22.00
Published on Web 10/12/2002

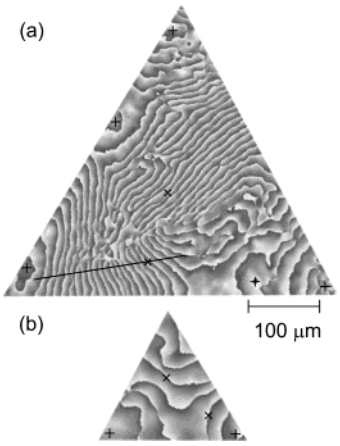

Figure 1. Typical morphologies of a (111) face of a ferritin crystal. Phase-wrapped images resulting from the convolution of five images recorded with an increasing phase shift as discussed in the text. The intensity of the gray color of a pixel is proportional to the average value of the *z*-coordinate, perpendicular to the image plane, over the surface area represented by this pixel. The height difference between adjacent gray-level discontinuities is $\lambda_{laser}/4n = 0.119$ μm, see text. (a) $\sigma = 4.3$, (b) $\sigma = 4.0$. +, location of layer generation; ×, locations of growth kinetics monitoring, solid line indicates locations of surface features quantification discussed further in the text.

converted into displacement of the face at this location. Care is taken to deconvolute the face displacement due to growth from the displacement due to thermal expansion or shrinking of the interferometer. For the *R* trace, the individual face displacement traces are differentiated with respect to time, the *p* traces are obtained as the ratio between the height difference to the distance between the two locations as a function of time, while v is computed as the ratio R/p. These data collection and processing routines are discussed in detail in ref 7.

II.3. Quantification of the Surface Morphology. Figure 1 shows phase-wrapped images representing the morphology of (111) faces of two ferritin crystals with sizes 470 and 200 μm. Each image is obtained from a sequence of five interferograms of the crystal surface recorded within 1 s with phase shift $\pi/2$ between them; the underlying assumption is that the surface does not change within this time period. Details about the image processing algorithms and the tests and calibrations are provided in ref 16. The gray scale in the images in Figure 1 is proportional to the surface height. The discontinuities result from the calculation algorithm based on the $\tan^{-1}$ function and correspond to a height difference of $\lambda_{laser}/4n$, where $\lambda_{laser} = 0.6328$ μm is the wavelength of the He−Ne laser used and $n = 1.3320$ is the refractive index of the solution, largely determined by its acetate and $CdSO_4$ components.[18]

III. Results and Discussion

III.1. Phenomenology of the Time-Dependent Kinetics. During the growth of ferritin crystals the growth layers are always generated by two-dimensional (2D) nucleation; for reviews on this and alternative mechanisms see, e.g., refs 19−23. For small crystal sizes and supersaturations $\sigma < 3$, the distribution of 2D nuclei is uniform across the whole face, and on a macroscopic scale, the face remains flat as the crystal grows. For higher supersaturations and crystals larger than 100 μm, 2D nucleation localizes at the facet edges and corners. Numerical modeling of diffusive-convective transport of crystallizing proteins has linked this localization to higher interfacial supersaturation at the edges.[24] Furthermore, the model calculations showed that the nonuniformity in interfacial supersaturation increases with the size of the crystal and the bulk solution supersaturation.

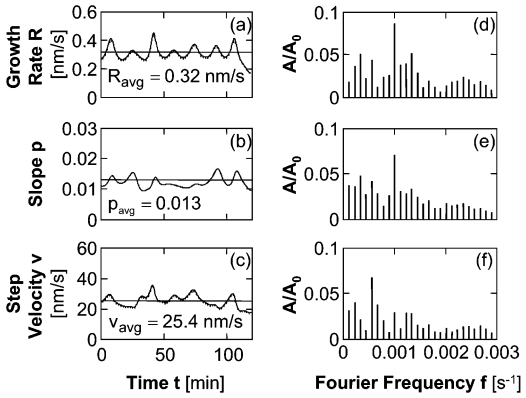

Figure 2. (a)−(c) Time traces of the normal growth rate *R*, the local slope *p* and the step velocity v recorded during growth of ferritin crystal at supersaturation $\sigma = 4.3$. (d−f) corresponding normalized Fourier spectra, for definitions, see text; in (d−f), the zeroth normalized amplitude, $A/A_0 = 1$ at $f = 0$ is omitted.

Figure 2a−c shows the time traces of the normal growth rate *R*, local slope *p*, and step velocity v recorded at the marked location near the facet center in Figure 1a at $\sigma = 4.3$. The *R*, *p*, and v fluctuate by up to 100% of their respective average values. The fluctuations of local slope, which is proportional to the step density, indicate that the unsteadiness occurs through the formation of patterns of lower and higher step density, step bunches. To analyze the fluctuations dependencies on different factors, such as supersaturation, crystal size, and location on the facet, we use Fourier decomposition of the three time traces. Earlier work has shown that the Fourier frequencies, characterizing the fluctuation time scales, and the Fourier amplitudes, corresponding to the deviations from average values of the respective kinetic variables, are reproducible characteristics of the unsteady behavior and only depend on the external conditions.[9] We use the Fourier transform in the form

$$R(t) = \sum_m A_m \cos\left(\frac{2\pi m}{T}t + \varphi_m\right), \quad m \geq 0 \qquad (1)$$

where A_m, $2\pi m/T = f_m$, and φ_m are the *m*th ($m = 0, 1, ...$) Fourier amplitude, frequency, and phase, respectively, and *T* is the total length of the monitoring period. All A_m's have the dimension of the growth rate *R* and A_0 equals the averaged growth rate, R_{avg}. The Fourier spectra of the time traces of local slope $p(t)$ and step velocity $v(t)$ are calculated in an equivalent fashion. Figure 2d−f presents the normalized Fourier spectra $A(f_m)/A_0$ of $R(t)$, $p(t)$, and $v(t)$. The Fourier frequencies are inversely proportional to the characteristic time scale Δt of the fluctuations.

III.2. Step−Step Interactions. Figure 2d−f show that the Fourier spectra for *R*, *p*, and v are similar. In particular, the *R* and *p* spectra reach their maximum amplitudes at the same frequency $f = 0.001$ s^{-1}, which corresponds to a fluctuation with $\Delta t \cong 17$ min. Since the Fourier spectra of *p* directly reflect the step bunching, we will use only these spectra in the further considerations.

As shown in Figure 2a−c, the fluctuations are rather periodic. However, there appears to be no correlation between the fluctuations of the slope and the step velocity. For further insight, we apply to following considerations. The dependence of step velocity on local slope and the reduced concentration (C −

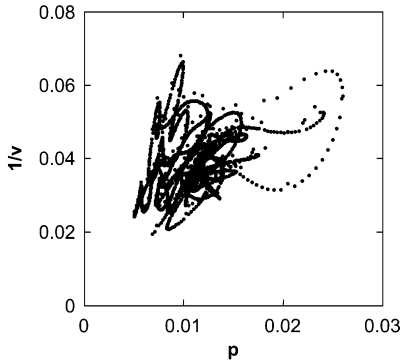

Figure 3. The correlation between the reciprocal local step velocity $1/v$ and the local slope p for the time traces recorded at the locations near the center of facet shown in Figure 1a over a period of several hours.

$C_e)C_e^{-1}$ can be expressed in a very generic form as[25]

$$v = \frac{b_{step}(C - C_e)/C_e}{1 + kp} \qquad (2)$$

where b_{step} is an effective step kinetic coefficient and k is a parameter characterizing the step−step interactions. For noninteracting steps, $k = 0$; for strongly interacting steps such as those in lysozyme growth, where incorporation into steps is preceded by slow diffusion through the solution bulk and the terraces between the steps, k is in the range 1000−2000;[8,25] for the growth of inorganic phosphates with a similar growth mechanism, values of k are ∼1000.[26,27]

Prompted by the form of the $v(p)$ dependence in eq 2, in Figure 3, we plot the reciprocal step velocity $1/v$ as a function of the local slope p for a trace recorded over several hours at the location near the center of facet in Figure 1a. In this presentation, steady p and v would be represented by a point; a deterministic proportionality between unsteady p and v^{-1} would appear as oscillations along a straight line. Deviations from the straight line indicate the action of a third factor that introduces a constant delay the response of v to p or p to v. As suggested from data for lysozyme,[8] the slow supply of protein from the solution bulk to the interface is the most likely cause of such phase delay. In the case of unchanging delay, the phase plot in $v^{-1}(p)$ coordinates would appear as an ellipse. The main axis of this ellipse would represent the deterministic dependence of $v^{-1}(p)$ that would be recorded if supply to the interface were infinitely fast, i.e., at $C_{surface} = \text{const}$.

The data in Figure 3 do not have a consistent trajectory, suggesting the action of several stochastic and uncoordinated factors. Extrinsic factors of this type include the inevitable mechanical perturbations during the experiments in the laboratory. Intrinsic factors that are likely contributing are the random grouping of steps that leads to constant variations in the depletion layer and the local interfacial supersaturation. Thus, the dynamics of our system seem to be closer to a chaotic state, than to a state of oscillations between two well-defined levels, typical of the classical flow instability patterns.[28]

The cloud of data in Figure 3 are randomly distributed and do not appear to oscillate around any deterministic and $v^{-1}(p)$ dependence. Such dependence would be an indication of a step−step interaction at close separations between the steps, corresponding to high p's.[25,26,29−33] The lack of such correlation indicates a very weak interaction between steps, i.e., the diffusion supply fields around the steps do not overlap. This makes the ferritin system quite different from lysozyme, which is characterized by strong interaction between steps, which results in dependence of step velocity on slope.[25]

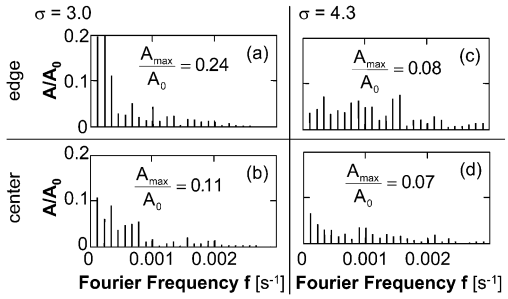

Figure 4. Fourier spectra of traces of the local slope p for the crystal of a 470 μm size shown in Figure 1a. (a) $\sigma = 3.0$, monitoring location at the facet edge, $p_{avg} = 0.006$; (b) $\sigma = 3.0$, monitoring location near the facet center, $p_{avg} = 0.008$; (c) $\sigma = 4.3$, edge, $p_{avg} = 0.012$; (d) $\sigma = 4.3$, center, $p_{avg} = 0.014$.

III.3. Variations of the Fluctuation Patterns with the External Conditions. Figure 4 presents the Fourier spectra of slope traces recorded at two locations on the facet shown in Figure 1a. The maximum values of the Fourier amplitudes are shown on the plots. Comparison of the spectra shows that the fluctuation amplitudes decrease as supersaturation increases and are greater near the facet edges than at the facet center. Note that the lower fluctuations at the facet center and at the higher supersaturations occur despite being accompanied by higher average vicinal slope. This is a remarkable observation, because the average vicinal slope has been identified as a major *destabilizing* factor for equidistant step trains.[34] We conclude that the mechanism leading to decay of the fluctuations is sufficiently strong to overpower the average slope effects.

To understand the higher p values at the facet center than at the facet periphery, see Figure 1a, we note that this interface shape is a result of the facet morphology response to nonuniform nutrient supply,[35] discussed in detail for the case of protein growth in refs 25 and 36. The nonuniformity in local step density compensates nonuniformity in interfacial supersaturation and step velocity. As a result, the normal growth rate R retains uniformity across the facet and the macroscopic flatness of the facet is preserved.

If we compare the steepest segments of a step train away from the crystal edge to the shallowest close to the edge, for instance along the line in Figure 1a, we would find a ratio of at most two. This ratio equals the ratio of the interfacial concentration of ferritin at the two locations, calculated in ref 24, i.e., the slope nonuniformity is completely determined by the surface concentration nonuniformity. This is in sharp contrast to findings with lysozyme, where a 10% surface concentration nonuniformity results in a 4−5× steeper slopes.[25,36] The strong enhancement of the surface morphology response was attributed to the strong step−step interaction in lysozyme; the observations with the weakly interacting steps on ferritin lend strong support to this mechanism.

In Figure 5, we compare the Fourier spectra of slope traces recorded at the center of two facets with different size at the same supersaturation $\sigma = 4.0$. The maximum amplitude value is significantly higher for the smaller crystal, while the averaged slope is lower in this case.

Figure 6 presents Fourier spectra of slope traces recorded simultaneously at two different locations of the facet shown in Figure 1b. The first location is close to the location of layer generation near the facet corner, while the second is further removed from the layer source. The amplitude of the slope

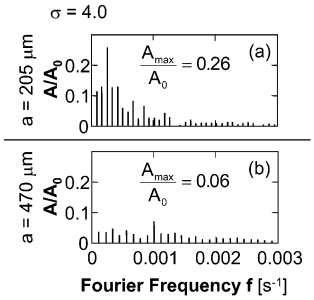

Figure 5. Decrease of the fluctuation amplitudes with a crystal size. $\sigma = 4.0$, crystal size a is indicated in each plot. (a) $p_{avg} = 0.005$; (b) $p_{avg} = 0.013$.

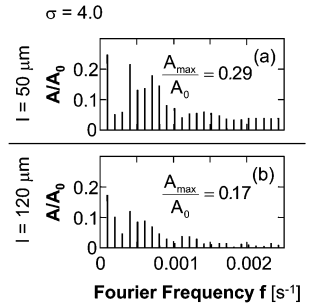

Figure 6. Normalized Fourier spectra of the p traces for the crystal of a 200 μm size shown in Figure 2a at $\sigma = 4.0$. (a) monitoring location is near layer source, $p_{avg} = 0.004$; (b) monitoring location is far from layer source, $p_{avg} = 0.008$. Fluctuation amplitudes decrease with distance l from layer source.

fluctuations decreases with the distance from layer source, while, as above, the averaged value of the slope increases.

To understand these observations, we use that the crystal size, the location on the facet and the supersaturation are parameters that strongly affect the solute supply to the interface. Hence, the observed dependencies of the fluctuation amplitudes with these parameters indicate that, similar to lysozyme,[8,9] the growth instability is due to the coupling of the nonlinear interfacial processes of growth to the bulk transport in the solution.

However, in all of the cases illustrated by Figures 4-6, the dependence of the fluctuation amplitudes on the respective parameter is opposite to that for lysozyme, and may appear counterintuitive. Thus, we would expect the faster growth at higher supersaturations to be more instable and with stronger fluctuations, we would expect the instabilities to evolve as the steps propagate down their pathway, and so on. This last controversy provides the key to understanding the unsteady behavior of the step trains in ferritin growth. Indeed, if the fluctuation amplitudes are dampened as the steps move on, it follows that the stable state, toward which the step train is converging, is the equidistant step train. Along this line of thought, we must conclude that the step bunches are generated at the location of step generation, i.e., the 2D nucleation process is highly unsteady, and consist of spurts of nucleated layers, leading to stacks of steps, followed by lower activity. The dependence of the fluctuation amplitudes on the supersaturation in the solution bulk suggests that the unsteady layer generation is caused by its coupling to the solute supply to the location of step generation. This coupling makes the nucleation process intrinsically unstable—an increase in the layer generation leads to solution depletion, a strong drop in the 2D nucleation rate, fewer nucleated steps that allow replenished supersaturation, and so on.

To test this model of nucleation caused step bunching, we expanded the model of coupled bulked transport and interfacial kinetics processes, discussed in ref 24 to include layer generation and step propagation.[24] The simulations results confirmed the suspected highly unsteady generation of layers at the facet edges.

The nonuniform step generation at the facet edges produces the step bunches. As the steps move away from their sources toward the facet center, the step bunches decay. An important factor for this decay is the lack of step−step interactions, reflected in the data in Figure 3—such interactions are known to strongly destabilize the uniform step trains, and lead to increasing fluctuations.[37]

Another potential destabilizing factor is impurity action. The main impurities in this system are the covalently bound ferritin dimers.[15] Previous work by AFM has found that, despite their relatively high surface concentration, $\sim 2.2 \times 10^9$ cm^{-2} ref 14, the dimers do not affect the motion of steps.[38] The reason for this is that the mean distance between two dimer molecules adsorbed on the surface, $\sim$200−300 nm, is higher than the critical 2D radius, of the order of several molecular diameters, i.e., 50−100 nm.[38−40] As a consequence, the dimers do not affect step motion, and do not enhance step bunch formation.

Since neither of these potential destabilizing mechanisms is acting, the motion of steps and the evolution of the step bunches formed at the stage of layer generation is only affected by the coupled bulk transport and surface kinetics. To identify which of the two coupled processes dominate the rate control, we evaluate the kinetic Peclet number, introduced in refs 8, 9, and 41 as the ratio

$$Pe_k = \beta p \delta / D \tag{3}$$

where D is the diffusivity of the ferritin $= 3.2 \times 10^{-7}$ cm^2/s ref 42, and δ is the characteristic diffusion layer thickness, typically of the order of 200 μm. Using the values of $\beta = 6 \times 10^4$ cm/s[17] and p discussed above, we get $Pe_k \approx 1.0$, i.e., ferritin grows under comparable control for transport in the solution and the interfacial kinetics. For such systems, the rationale put forth in refs 8, 9, 37, and 41 predicts higher stability at *even higher* relative weight of transport. Thus, we should expect lower kinetic fluctuations at higher supersaturations, at larger crystals sizes, and at the facet centers. This is in exact correspondence with the experimental findings discussed above. We conclude that the observations with ferritin support the mechanism of generation of the step bunches and the associated rationale for the control of the kinetics instabilities in layer growth systems put forth in refs 8, 9, 12, 37, and 41.

III.4. Spatiotemporal Characteristics of the Step Patterns. The phase-shifting technique allows reconstruction of the surface morphology. Figure 7a shows the height profile along the line depicted in Figure 1a. The height decreases as the distance from layer sources increases. The corresponding slope profile and its spatial Fourier spectrum are shown in Figure 7b,c, respectively. The wavenumbers in Figure 7c are reciprocal to the corresponding step bunch wavelengths λ. The maximum amplitude occurs at a wavenumber of 0.045 μm^{-1} corresponding to fluctuations with $\lambda_{max} \sim 21$ μm. From the time traces measured at the location on profile line at the same $\sigma = 4.3$, see Figure 4c, we determine the characteristic step bunch frequency $f_{max} = 0.0016$ s^{-1} ($\Delta t \sim 10.7$ min). From these two values, we can evaluate the step bunch velocity as $v_{bunch} \approx \lambda_{max} f_{max} \sim 33$ nm/s. The value of v_{bunch} is close to mean step velocity under those conditions, $v \approx 35$ nm/s. Thus, in the case of noninteracting steps, the step bunches move with the same velocity as elementary steps.

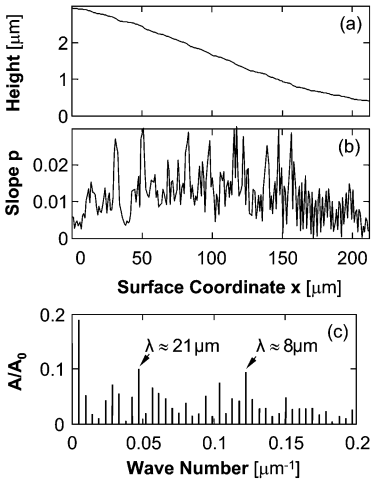

Figure 7. (a) Height and (b) local slope profiles along the line shown in Figure 1a. (c) Corresponding Fourier spectrum of p. The characteristic step bunch wavelengths λ are indicated in the plot. The first amplitude in (c) corresponds to the overall bending of the surface seen in (b).

IV. Conclusions

We have shown that under steady growth conditions, ferritin growth kinetics is highly unsteady and the fluctuation amplitudes reach up to 100% of the average values of the growth rate, the step density and the step velocity. The variations in local slope indicate that the fluctuations reflect the dynamics of formation and evolution of step patterns. The lack of correlation of the step velocity and local slope indicates very weak step−step interactions. Correspondingly, the propagation rate of step bunches is same as elementary step velocity.

From the dependencies of the amplitude of local slope fluctuations on the supersaturation, crystal size and location on the facet we conclude that the unsteady growth is the result of the coupling between solute transport toward the interface and the nonlinear interfacial kinetics. The main factor introducing nonlinearity onto the interfacial kinetics is the generation of layers via a 2D nucleation mechanism, with its suspected exponential dependence on the supersaturation. We find that the fluctuation amplitude decreases with increasing distance from the layer sources. Hence, for noninteracting steps growing under diffusion control the step bunches decay and the step train tends toward its stable, equidistant state.

These findings in a transport-controlled system provide a strong support to the rationale for the control of the step bunching instabilities in layer growth systems that was previously based only on observations with a kinetically controlled system.

Acknowledgment. We thank Bill Thomas for purification and analysis of the protein solutions used in this work, Nicholas Booth for help with the interferometry setup, Kai Chen for supplementary AFM determinations, and Hong Lin for access to unpublished computational results. Research support by the Office of Biological and Physical Research, NASA (Grant NAG8-1857) is gratefully acknowledged.

References and Notes

(1) Burley, S. K.; Almo, S. C.; Bonanno, J. B.; Capel, M.; Chance, M. R.; Gaasterland, T.; Lin, D.; Sali, A.; Studier, F. W.; Swaminathan, S. *Nature Genetics* **1999**, *23*, 151.

(2) McPherson, A. *Preparation and Analysis of Protein Crystals*; Wiley: New York, 1982.

(3) McPherson, A. *Crystallization of Biological Macromolecules*; Cold Spring Harbor Laboratory Press: Cold Spring Harbor New York, 1999.

(4) Chernov, A. A. *Modern Crystallography III, Crystal Growth*; Springer: Berlin, 1984.

(5) Bauser, E. Atomic Mechanisms in Semiconductor Liquid-Phase Epitaxy. In *Handbook of Crystal Growth*; Hurle, D. T. J., Ed.; North-Holland: Amsterdam, 1994; Vol. 3b, p 879.

(6) Vekilov, P. G.; Rosenberger, F. *Phys. Rev. E* **1998**, *57*, 6979.

(7) Vekilov, P. G.; Monaco, L. A.; Rosenberger, F. *J. Crystal Growth* **1995**, *146*, 289.

(8) Vekilov, P. G.; Alexander, J. I. D.; Rosenberger, F. *Phys. Rev. E* **1996**, *54*, 6650.

(9) Vekilov, P. G.; Thomas, B. R.; Rosenberger, F. *J. Phys. Chem.* **1998**, *102*, 5208.

(10) Schwoebel, R. L.; Shipsey, E. J. *J. Appl. Phys.* **1966**, *37*, 3682.

(11) Ehrlich, G.; Hudda, F. G. *J. Chem. Phys.* **1966**, *44*, 1039.

(12) Vekilov, P. G.; Alexander, J. I. D. *Chem. Rev.* **2000**, *100*, 2061.

(13) Yau, S.-T.; Petsev, D. N.; Thomas, B. R.; Vekilov, P. G. *J. Mol. Biol.* **2000**, *303*, 667.

(14) Yau, S.-T.; Thomas, B. R.; Galkin, O.; Gliko, O.; Vekilov, P. G. *Proteins: Struct., Funct., Genet.* **2001**, *43*, 343.

(15) Thomas, B. R.; Carter, D.; Rosenberger, F. *J. Crystal Growth* **1997**, ***187***, 499.

(16) Gliko, O.; Booth, N. A.; Rosenbach, E.; Vekilov, P. G. *Crystal Growth Des.* **2002**, *2*, 381.

(17) Chen, K.; Vekilov, P. G. *Phys. Rev. E* **2002**, *66*, 021606.

(18) Fredericks, W. J.; Hammonds, M. C.; Howard, S. B.; Rosenberger, F. *J. Crystal Growth* **1994**, *141*, 183.

(19) McPherson, A.; Malkin, A. J.; Kuznetsov, Y. G. *Structure* **1995**, *3*, 759.

(20) Malkin, A. J.; Kuznetsov, Y. G.; Land, T. A.; DeYoreo, J. J.; McPherson, A. *Nature Struct. Biol.* **1996**, ***2***, 956.

(21) Malkin, A. J.; Kuznetsov, Y. G.; Glanz, W.; McPherson, A. *J. Phys. Chem.* **1996**, ***100***, 11736.

(22) Kuznetsov, Y. G.; Malkin, A. J.; McPherson, A. *J. Crystal Growth* **1999**, *196*, 489.

(23) McPherson, A.; Malkin, A. J.; Kuznetsov, Y. G.; Plomp, M. *Acta Crystallogr., Sect. D* **2001**, *57*, 1053.

(24) Lin, H.; Petsev, D. N.; Yau, S.-T.; Thomas, B. R.; Vekilov, P. G. *Crystal Growth and Design* **2001**, *1*, 73.

(25) Vekilov, P. G.; Monaco, L. A.; Rosenberger, F. *J. Crystal Growth* **1995**, *156*, 267.

(26) Vekilov, P. G.; Kuznetsov, Y. G.; Chernov, A. A. *J. Crystal Growth* **1992**, *121*, 643.

(27) Booth, N. A.; Chernov, A. A.; Vekilov, P. G. *J. Crystal Growth* **2002**, *237*−*239*, 1818.

(28) Cross, M. C.; Hohenberg, P. C. *Rev. Mod. Phys.* **1993**, *65*, 851.

(29) Bostanov, V.; Staikov, G.; Roe, D. K. *J. Electrochem. Soc.* **1975**, *122*, 1301.

(30) Gratz, A. J.; Hillner, P. E.; Hansma, P. K. *Geochimica and Cosmochimica Acta* **1993**, *57*, 491.

(31) Hillier, P. E.; Manne, S.; Hansma, P. K.; Gratz, A. J. *Faraday Discuss.* **1993**, *95*, 191.

(32) DeYoreo, J. J.; Land, T. A.; Dair, B. *Phys. Rev. Lett.* **1994**, *73*, 838.

(33) Land, T. A.; DeYoreo, J. J.; Lee, J. D. *Surf. Sci.* **1997**, *384*, 136.

(34) Chernov, A. A.; Coriell, S. R.; Murray, B. T. *J. Cryst. Growth* **1993**, *132*, 405.

(35) Chernov, A. A. *J. Crystal Growth* **1974**, *24/25*, 11.

(36) Lin, H.; Vekilov, P. G.; Rosenberger, F. *J. Crystal Growth* **1996**, *158*, 552.

(37) Vekilov, P. G.; Lin, H.; Rosenberger, F. *Phys. Rev. E* **1997**, *55*, 3202.

(38) Yau, S.-T.; Thomas, B. R.; Vekilov, P. G. *Phys. Rev. Lett.* **2000**, *85*, 353.

(39) Yau, S.-T.; Vekilov, P. G. *Nature* **2000**, *406*, 494.

(40) Yau, S.-T.; Vekilov, P. G. *J. Am. Chem. Soc.* **2001**, *123*, 1080.

(41) Vekilov, P. G.; Rosenberger, F. *Phys. Rev. Lett* **1998**, *80*, 2654.

(42) Petsev, D. N.; Thomas, B. R.; Yau, S.-T.; Vekilov, P. G. *Biophys. J.* **2000**, *78*, 2060.